Spin Waves in Ferromagnetic CrBr₃ Studied by Inelastic Neutron Scattering

E. J. Samuelsen, * Richard Silberglitt, and G. Shirane

Brookhaven National Laboratory,[†] Upton, New York 11973

and

J. P. Remeika

Bell Telephone Laboratories, Murray Hill, New Jersey 07974

(Received 27 July 1970)

Neutron scattering measurements of spin waves in a nonmetallic ferromagnetic material are reported here for the first time. CrBr₃ is a rhombohedral two-sublattice ferromagnet below $T_C = 32.5$ °K, and we have observed acoustical and optical spin waves at 6 °K as well as investigated their temperature behavior. The dispersion relation is found to be highly directionally dependent, being very flat along the hexagonal c direction, thus verifying directly previous conclusions obtained from magnetization data. The intralayer ferromagnetic coupling is dominated by the nearest-neighbor interaction, and the much weaker interlayer coupling results from competing ferromagnetic and antiferromagnetic interactions. The use of a two-parameter model is only qualitatively correct, except for the low-energy part, where quantitative description to within 5% accuracy is possible by two parameters only. In the study of the temperature effects, the particularly interesting observation was made that the spin-wave energy renormalization is also directionally dependent. Such an effect has not been observed previously since it is negligibly small for cubic or nearly cubic systems. The effect represents the first direct evidence in favor of Dyson's dynamical spin-wave theory. In fact, energy shifts calculated using this theory were found to be in quantitative agreement with observations up to a temperature of about 0.8 T_C. As T_C is approached, the widths of the spin-wave peaks increase, and the peaks disappear at T_C by broadening out at finite energies. Well-defined spin waves were not seen above T_C.

I. INTRODUCTION

The Heisenberg model is now broadly accepted for the description of magnetism in solids with localized unpaired electrons.[1,2] Most nonmetallic magnetic materials order antiferromagnetically at sufficiently low temperatures and the Heisenberg model has been successfully applied to many of them, although there are some theoretical difficulties involved in the question of the proper ground state in the antiferromagnetic case.[2] No such difficulty exists for a ferromagnet, and numerous theoretical papers have appeared on various aspects of Heisenberg ferromagnetism.[3] Unfortunately, only very few nonmetallic ferromagnetic materials exist on which these theories may be tested.

Neutron scattering investigation is of course known as one of the most powerful means of obtaining direct information on basic magnetic properties,[4] but in the case of the few nonmetallic ferromagnetic materials that do exist, either single crystals of sufficient size have not been readily available, or the materials are neavy neutron absorbers, like EuO and EuS. Accordingly, no neutron studies of spin waves in nonconducting ferromagnets have previously been reported.

Tsubokawa[5] discovered in 1960 that CrBr₃ orders ferromagnetically below about 35 °K. NMR mea-

surements by Gossard, Jaccarino, and Remeika[6] and later by Davis and Narath[7] furnished a very accurate determination of magnetization vs temperature, which were interpreted by means of spin-wave theories of various degrees of sophistication.[6-8] The interesting conclusion was reached that the magnetic coupling is much stronger within the hexagonal layers of Cr³⁺ ions than between the layers, giving CrBr₃ some character of a two-dimensional system. The weak interlayer coupling makes the excitation spectrum in the hexagonal c direction very flat, which in turn requires a proper treatment of spin-wave interactions for the interpretation of the magnetization data.[7,8] Since the actual values of the Heisenberg coupling parameters derived from the magnetization data depend upon the details of these treatments, a direct observation of the spin-wave spectrum by neutron scattering would not only furnish a test on the derived parameters, but also yield a test of the interaction calculations behind them. Furthermore, neutron measurements could give information about the entire spin-wave spectrum rather than only the low-energy part obtained from the NMR data.

As we succeeded in growing a sample of the material of fair quality and reasonable size, such a neutron experiment was undertaken. In the following text the relation between the NMR results and the low-energy spin waves is established and
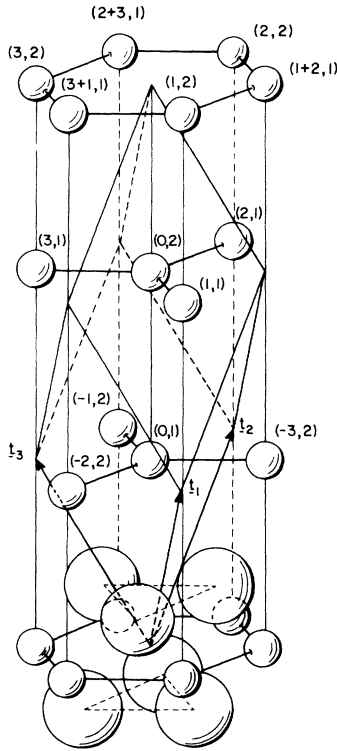
FIG. 1. The rhombohedral unit cell and some details of the atomic arrangement in $CrBr_3$. Small balls: Cr^{3+} ions. Large balls: Br^- ions. Each Cr^{3+} layer has a layer of Br^- ions on either side, but for clarity only one such "sandwich" is shown (bottom). The labeling $(n,\ j)$ of the Cr^{3+} ions refers to unit cell (n) and sublattice (j) relative to the unit cell shown with the lattice vectors $\vec{t}_1$, $\vec{t}_2$, and $\vec{t}_3$. The same notation is used in Table I.

we report the observation of the dispersion relation over the entire Brillouin zone (BZ) and the tempera- dependence of the spin-wave excitations.

II. CRYSTAL STRUCTURE AND SPIN-WAVE DISPERSION RELATION

$CrBr_3$ has the BiI_3-type crystal structure which belongs to the rhombohedral space group C_{3i}^2 $(R\bar{3})$. Although it may conveniently be described by a hexagonal unit cell, we shall use the smaller rhom- bohedral unit cell which contains two Cr^{3+} ions and has dimensions $a = 7.062$ Å and $\alpha = 52.62°$, as cal- culated from the hexagonal dimensions determined by Braekken.[9] The atomic positions are not ac- curately known, but the Cr^{3+} atoms are probably little removed from the ideal $\frac{1}{3}\frac{1}{3}\frac{1}{3}$ position[10] and therefore form an almost ideal honeycomb layer structure, where each layer is shifted one inter- ionic distance relative to its neighboring layers. The unit cell and some details of the ionic arrange- ment are shown in Fig. 1. For clarity, only two of the Br^- layers are included. They are such that

each Cr^{3+} ion finds itself with an almost perfect octahedral coordination.[10]

In Table I, we list some of the first-nearest- neighbor pairs and define the corresponding inter- action constant J_m, where m increases (from 1) for increasing interionic distance. Previous treat- ments of the exchange interactions in $CrBr_3$ have been on a simplified model,[6,7] where the interlayer interactions $(J_1, J_4, J_5,$ and $J_7)$ were substituted by one effective constant J_L, and the intralayer param- eters $(J_1, J_3,$ and $J_6)$ by one effective J_T. Such an approximation has the definite advantage of making the mathematical treatment of spin-wave inter- actions feasible.[7] It also furnishes a fairly good description of the low-energy part of the spin-wave spectrum, although there are some limitations to it as discussed later in Sec. VI. For the purpose of comparison, we shall interpret our low-energy spin-wave data by the simplified hexagonal model (in addition to using the proper BiI_3 structure). The dispersion relation for spin waves in that lattice has been given previously,[7] and in the Appendix we reproduce the expressions for propagation along the [111] axis and for two directions in the (111) plane. There is no reason, however, to expect the two-parameter model to fit the entire observed spin-wave spectrum.

The dispersion relation for spin waves in a ferro- magnet with the BiI_3 lattice is also given in the Appendix, as derived by standard procedures.[11] An isotropic Heisenberg Hamiltonian was used, in-

TABLE I. Definition of interaction parameters J_m between the seventh nearest neighbors. The ion-pair labeling $(n,j)-(n',j')$, where n, n' label the unit cells and j, j' the sublattices, refers to Fig. 1. The interionic vectors are defined through the rhombohedral lattice vectors $\vec{t}_1$, $\vec{t}_2$, $\vec{t}_3$ and $\vec{Z} = \vec{t}_1 + \vec{t}_2 + \vec{t}_3$. ρ_{12} $(\approx \frac{1}{3})$ is the frac- tional distance between sublattices 1 and 2 within the same unit cell. The three first interactions of the table are between ions in the same hexagonal layer, the four last ones are between ions in adjacent layers.

Exchange interaction	Ion pair	Number of neighbors	Cr-Cr distance	Interionic vectors
J_n	$(n,j) - (n',j')$		Å	
J_1	$(0,2) - (2,1)$	3	3.62	$\vec{t}_i - \vec{Z}\rho_{12}$
J_3	$(1,1) - (2,1)$	6	$6.26 \pm$	$(\vec{t}_i - \vec{t}_j)$, $i \neq j$
J_6	$(3,2) - (1+2,1)$	3	7.24	$\vec{t}_i + \vec{t}_j - \vec{t}_k - \vec{Z}\rho_{12}$, $i \neq j \neq k$
J_2	$(0,2) - (0,1)$	1	6.07	$-\vec{Z}\rho_{12}$
J_4	$(0,2) - (1+2,1)$	3	7.05	$\vec{t}_i + \vec{t}_j - \vec{Z}\rho_{12}$, $i \neq j$
J_5	$(0,2) - (1,2)$	6	7.06	$\pm\vec{t}_i$
J_7	$(1,1) - (2,2)$	6	8.74	$\pm(\vec{t}_i - \vec{t}_j) + \vec{Z}\rho_{12}$, $i \neq j$

volving up to seven nearest-neighbor exchange param-
eters and an effective anisotropy field H_A, which
was assumed equal for the two sublattices. There
is good evidence, however, from Bené's pair mea-
surements[12] of Cr^{3+} in BiI_3, that the nearest-neighbor
interaction J_1 is considerably anisotropic, and Bené
shows that the largest contribution to H_A is in fact
from this anisotropy. After performing the neces-
sary coordinate transformations of Bené's pair
Hamiltonian[12] and invoking the threefold symmetry
of the lattice, the spin-wave dispersion relation was
also derived for the anisotropic case, using the
general formalism given by Lindgård et al.[13] Since
the expressions are rather lengthy and failed to
bring about very much of an improvement of the fit
with experiments, they are not reproduced here.
The anisotropic part in fact enters the energy expres-
sions in such a form that distinction from the iso-
tropic case is not possible from energy measure-
ments alone, unless the anisotropy is made un-
realistically large.

III. SAMPLE

Crystals of $CrBr_3$ were grown by the method
originally devised by Tsubokawa.[5] Chromium metal
powder placed near the end of a closed quartz tube
furnace was heated to 850 °C in an atmosphere of
Br_2, and in the course of three days crystals were
obtained at the opposite end of the tube, which was
held at 600 °C. The best piece obtained as deter-
mined by neutron-diffraction investigation was in
the form of a triangular plate of dimensions 21×14
$\times 4$ mm^3. It turned out to consist of several inter-
grown single cyrstals, all of which had the hexagonal
c axis in common. Careful scans with a small
neutron probe across the sample did not reveal any
spatial separation of the various single crystals.
We shall refer to the different single crystals as
different domains. In turning the sample around the
c axis the domains were distinguished by the ap-
pearance of their rhombohedral $1\bar{1}0$ reflections as
shown in Table II. Each of the three reflections
shown there of course reappeared with a periodicity
of 60°. It further turned out that each domain was
twinned about the c plane. This twinning will be
denoted by the letters a and b.

TABLE II. The multicrystallinity ("the domains") of
the sample as determined from detecting the rhombo-
hedral ($1\bar{1}0$) reflection while turning the sample around
the [111] axis.

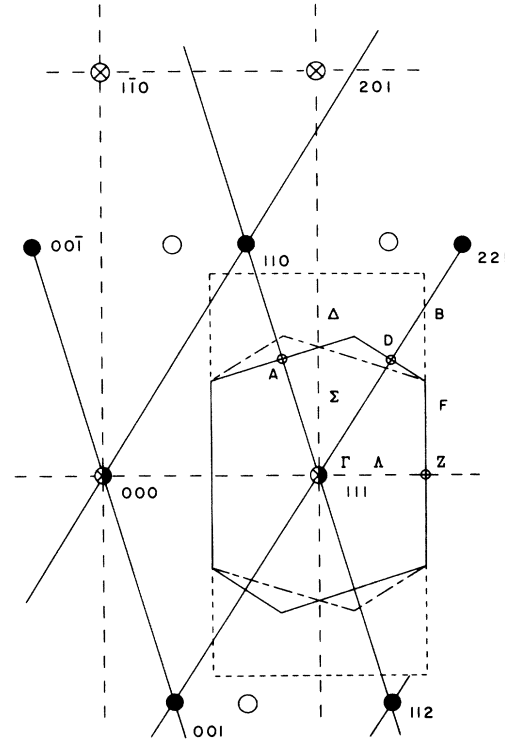| Turning angle from domain I	Relative neutron intensity	Assigned domain label
0°	1	I
30.8°	1	II
35.4°	0.5	III

FIG. 2. Superposition of the ($1\bar{1}0$) and the ($11\bar{2}$) planes
of the reciprocal space. The ($1\bar{1}0$) planes refer to
domain I of the sample, the filled and open lattice points
belonging to the twins I_a and I_b. Three directions are
equivalent for the twins: the directions Λ (or [111] or
c axis), Σ (or the c plane through Γ), and F (or the
c plane through Z). The ($11\bar{2}$) plane refers to domain
II. It has the Λ direction in common with domain I.
The c plane directions Δ (through Γ) and B (through Z)
for domain II are indicated. The labeling of points and
directions is in accordance with Koster (Ref. 14) and is
used in subsequent figures and in the text.

The individual reflections from the sample, in-
cluding the hhh reflections, were all well shaped
and had a full width of half-maximum of the order
of 0.3°.

The sample was mounted on the spectrometer with
the [$1\bar{1}0$] zone axis of domain I vertical. The re-
ciprocal plane of this zone is shown in Fig. 2 as the
fully-drawn net with filled reciprocal-lattice points
for I_a and open points for I_b. The orientation of
domain II is then 0.8° from having the [$11\bar{2}$] zone
axis vertical, and the equatorial reciprocal plane
of the [$11\bar{2}$] zone has therefore been included in
Fig. 2 as the dashed net. The a, b twinning does
not enter for this plane. Domain III will nearly
coincide with domain II, and since it is of lower
intensity, it has not been further considered. The
Brillouin zones of domains I_a, I_b, and II are in-
dicated in Fig. 2 around the 111 reciprocal-lattice

point where most of the measurements were per-
formed.

The fact that the sample was a multicrystal may
at first glance look like at least a very unpleasant
complication. However, as it turned out, mea-
surements on the two different zones shown in Fig.
2 could be carried out simultaneously. First of
all, since the Λ direction ([111] axis) is common,
data taken along that direction are unambiguous.
Further, the vicinity of this axis is cylindrically
symmetric due to the threefoldness of the axis,
and for that region contributions from the different
domains must coincide. Sufficiently far removed
from the [111] axis, domains I and II would be ex-
pected to split, since their zone boundaries are
located differently. Once domain II is split out, it
can be studied all over the zone because the a, b
twinning does not affect it. And finally, domain I,
when split out from domain II, can be studied along
arrays in the (111) plane at levels Γ (Σ direction)
and Λ (F direction), where the a, b twins will re-
main degenerate.

IV. MEASUREMENTS

The measurements were performed on a triple-
axis spectrometer at the Brookhaven High Flux
Beam Reactor. Pyrolytic graphite monochromator
and analyzer crystals were used, and fixed incident
energies of the neutron beam of 5.2, 14, and 38
meV were chosen according to the range of spin-
wave energies being studied. For 5.2 and 15 meV
the beam was passed through a pyrolytic graphite
filter, which reduces the higher-order contamina-
tion.

The sample was glued onto a 0.5-mm-thick
Al plate and mounted in a temperature-controlled
liquid-He Dewar. The Curie point was determined
to 32.5 ± 0.5 °K by following the variation of the
neutron intensity of the rhombohedral (001) reflec-
tion with temperature. No magnetic contribution
to within 3% accuracy could be detected at any tem-
perature to the elastic (111) and (333) reflections,
which are nuclearly weak, showing that the spins
are directed along the [111] axis, in agreement with
the results of torque measurements.[5]

The inelastic measurements are naturally divided
into two parts: the observation of the spin-wave
dispersion relation at low temperature and the
study of temperature effects on the spin-wave energy.
These two parts are presented separately in the
following.

V. OBSERVATION OF SPIN-WAVE DISPERSION

The spin-wave dispersion relation was investi-
gated in detail at a temperature of 6 °K. Spin waves
were distinguished from phonons by the effect of
heating the sample to above the Curie point. As
described later the spin-wave scattering peaks

disappeared at T_C by broadening out.

Most measurements were carried out in the
vicinity of the (111) reciprocal-lattice point. As
it turned out, the energy measurements could be
carried out with unusually high precision, in parti-
cular for spin waves off the [111] axis, because of
favorable focusing conditions. It is well known that
focusing is achieved when the inclination of the in-
strumental probe in energy-momentum space ($\hbar\omega$-q
space) can be made to coincide with the local slope
of the dispersion relation.[15] The instrumental in-
clination varies with the energy of the incident
beam, and it so happened that focusing conditions
were very closely fulfilled over considerable energy
ranges explored with each of the three incident
energies. Some observed peaks shown in Figs.
3 and 4 illustrate this. Figure 3 shows peaks ob-
tained for incident energies 14 and 38 meV at the
same point in the reciprocal space, namely, in the
region where domain I and II split. The 14-meV
data show focused peaks for domain I and the 38-
meV data focusing for domain II, for which the
dispersion is steepest. Very-low-energy peaks are
shown in Fig. 4, where good focusing off the 111
axis is demonstrated. In the [111] direction no
focusing takes place but reasonably high accuracy
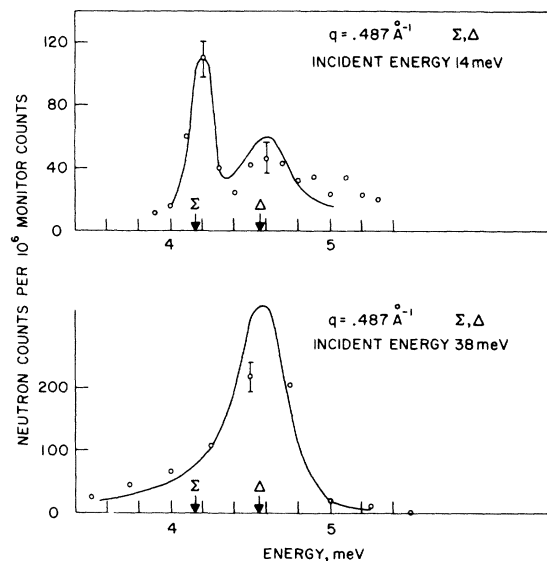is still attained due to the inherently higher resolu-

FIG. 3. Intensity profiles as measured and calculated
for constant wave vector with two different incident
neutron energies. 14-meV energy gives rise to focusing
of the spin-wave peak belonging to domain I, and 38 meV
focuses the spin-wave peak belonging to domain II. The
calculations were performed using the folding program of
Ref. 16. The arrows show the nominal energy of the spin
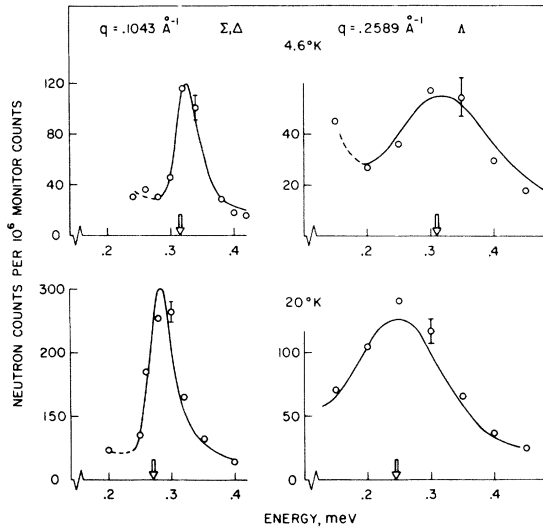waves used in calculating the curves.

FIG. 4. Intensity profiles for low–energy spin waves of the same energy along Σ, Δ and along Λ at 4.6 °K and 20 °K. The Σ, Δ peaks are well focused, giving rise to a high accuracy of the spin-wave energy. The renormalization of energy with temperature is demonstrated. Calculated profiles are shown, and arrows indicate the nominal energy of the spin waves entering the folding program (Ref. 16).

tion associated with the low incident energy of 5.2 MeV.

Some corrections due to instrumental resolution, effects are sometimes required of the neutron spectrometer data.[16] The corrections are normally of significance only for systems with steep dispersion relations and for nonfocused peaks. Some calculations were performed using a previously described program[16] to fold the instrumental resolution function with the scattering cross section. They revealed that for the high-energy end of the spectrum some minor corrections were needed for a few cases, the corrections always amounting to less than the experimental uncertainty. The curves shown in Figs. 3 and 4 are the calculated line shapes.

The observed dispersion relations are shown in Figs. 5 and 6. The thermodynamically important[7, 8] low-energy parts are given in Fig. 5, including the entire acoustical branch in the Λ direction. Figure 6 shows the data taken in directions normal to Λ. The labeling of the directions and points shown refers to Fig. 2. The three branches shown were assigned to domains I and II as indicated, based upon their apparent periodicity. Since $CrBr_3$ contains two Cr^{3+} ions per unit cell, an optical spin-wave branch is expected in addition to the acoustical, and it is shown in Fig. 6 for domain I(Σ, F directions). Optical spin waves have pre-

viously been observed in the ferrimagnet Fe_3O_4[17] and the antiferromagnet $\alpha\text{-}Fe_2O_3$.[18] One should notice the way in which the optical-branch data in Fig. 6 are presented, namely, at the points in reciprocal space relative to 111 where they were actually observed. The reason is that, if folded back to the 111 BZ, they would not include the points Γ and Z. The optical branch is not directly observable in the BZ surrounding 111 because of an almost vanishing structure factor, and when observed at the 001 or 110 reciprocal-lattice points with our samples, the peaks are not "clean," as a consequence at the a, b twinning.

No second branch due to domain II was seen. Calculations show that its dynamical structure factor nearly vanishes along the whole Δ direction. The two branches, in fact, cross at two-thirds distance to the zone boundary, but the structure factor allows only one continuous branch to be seen.

VI. LOW-ENERGY SPIN WAVES

The spin waves that are important thermodynamically in determining the magnetization deviation at a given temperature are, of course, those with an energy comparable to the thermal energy of the system. For temperatures below 20 °K this will imply spin waves of energy less than about 3 meV. The observed dispersion relation for some of those
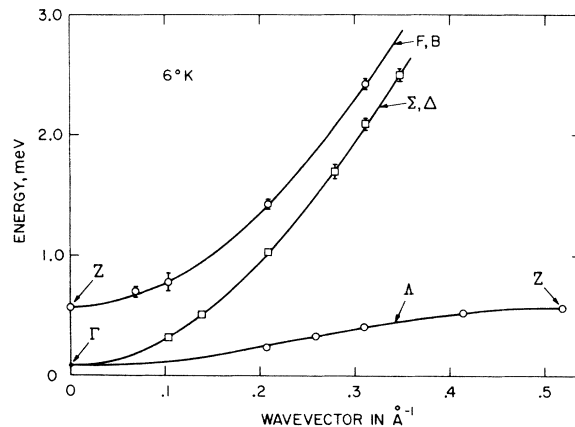

FIG. 5. Dispersion relation of spin waves of low energy as measured in various directions at 6 °K, all shown on the same abscissa. The labeling corresponds to that of Fig. 2. Where no error bars are given, the uncertainties are less than the size of the symbols. Notice that the F, B direction has its origin at the Z point of the Brillouin zone. This way of presenting the data is chosen (i) to show the large difference of stiffness along the c axis and in the basal plane and (ii) to demonstrate the difference between the Σ, Δ and the F, B curves, which bears a relation to the applicability of the two-parameter model. The curves are given by the three parameters discussed in Sec. VI, or equally well by fits 2 and 3 of Table III.
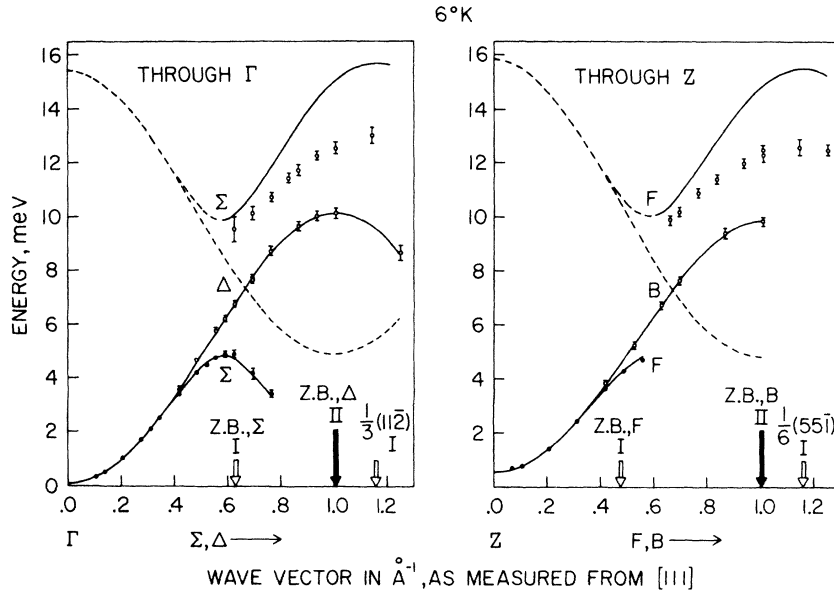
FIG. 6. Dispersion relation for spin waves at 6 °K for directions parallel to the c plane. The labeling corresponds to that of Fig. 2. Referred to the center of the BZ at the 111 reciprocal-lattice point, the spin waves are shown where they were actrally observed. The curves are those corresponding to fit 2 of Table III. They are shown as dashed in the regions where their dynamical structure factors for neutron scattering is vanishingly small, as found by calculations. The large discrepancy for the optical branch is noticed. See end of Sec. VII for discussion.

spin waves is shown in Fig. 5. The most striking feature of this figure is, of course, the very flat dispersion observed in the $\Lambda(c$-axis) direction as compared to directions normal to it. This is in excellent agreement with the picture deduced from the magnetization data.[6,7] Since the two-parameter lattice model was used previously in interpreting these data,[6,7] we shall in the following use it tentatively for parametrizing the neutron results.

For the Σ, Δ direction (the basal plane) a plot of the observed energies versus

$$[1 - \tfrac{1}{3}(5 + 4 \cos\tfrac{1}{2}\sqrt{3}\, a_H q)^{1/2}] ,$$

as suggested by Eqs. (A3) and (A4) of the Appendix, gives a straight line. A value of $J_T = 0.76 \pm 0.02$ meV can be determined from the slope, and the intersection at $q = 0$ gives a value of $E_g \equiv \mu g H_A$ $= 0.08 \pm 0.02$ meV. The latter value is in excellent agreement with 0.08 meV determined from Dillon's[19] ferromagnetic resonance measurements at 6 °K.[20] The Σ, Δ curve of Fig. 5 is drawn using these parameters.

However, when the F, B direction (basal plane through Z) is also considered, a shortcoming of the two-parameter model becomes evident. The model predicts identical curvature for the Σ, Δ and the F, B directions, but a similar treatment of the F, B data yields a value of $J_T = 0.70 \pm 0.02$ meV. This value was used to draw the F, B curve of Fig. 5. Since the value of J_T obtained from interpretation of the magnetization data is determined by some weighted averages over all directions in the BZ it should ideally fall somewhere between the two values here determined. This is in fact the case for the value $J_T = 0.711 \pm 0.011$ meV deduced by

Davis and Narath.[7]

Along the Λ direction one can fit the observed points very well by using 0.08 meV for the gap E_g with $J_L = 0.041 \pm 0.002$ meV, as shown by the Λ curve drawn in Fig. 5.

When this value is reduced to absolute zero temperature using calculated renormalization functions[7] (the corresponding correction for J_T is negligible) one finds $J_L = 0.043 \pm 0.002$ meV which compares favorably with the value of 0.0428 ± 0.0008 meV obtained from the magnetization data.[7] Thus, within the error introduced by the shortcoming of the two-parameter model there is excellent agreement between the two highly different methods of determining the exchange interactions in $CrBr_3$. As pointed out in Ref. 8, the actual values derived from the magnetization data, in particular for J_T, are somewhat dependent upon the treatment of the spin-wave interactions. Inclusion of repeated scattering events by summing the entire Born series to all orders in the interaction potential via the t matrix would require a slightly higher value than 0.711 ± 0.011 meV for J_T.[8,21] Unfortunately, because of the shortcoming of the two-parameter model, no conclusion on this point can be drawn from the neutron data.

In Sec. VII, the low-temperature spin waves will be included in a fit to the correct BiI_3 structure. The resulting fit with five parameters gives curves indistinguishable from those drawn in Fig. 5.

VII. DATA FITTING AND INTERACTION CONSTANTS

A least-squares fitting program was used in attempts to fit the theoretical dispersion relations

[Eqs. (A6)-(A20)] to the observations. It soon became clear that a good fit could not be obtained when all observations were included, regardless of the number of parameters. Best fits always showed systematic deviations outside the experimental uncertainties over considerable regions of the BZ. In particular, the fitted optical Σ branch tended to be too low at the zone boundary and too high near the zone center by half a millivolt or more, and a similar discrepancy occurred for the zone-boundary Δ part. Some parameters from such a fit, together with the value of the minimized function F_{min} are shown in Table III.

Inclusion of anisotropic exchange of the type discussed in Sec. II improved the fit very little. To investigate whether there is any systematic disturbance associated with any particular class of the experimental data, parts of the data were systematically excluded from the least-square fitting procedure. It then turned out that an excellent fit could in fact be obtained with the remaining data when the Σ, F optical branch was excluded. Other exclusions, such as the high-energy Δ part or the high-energy part of the Σ acoustical branch, did not give rise to a similarly satisfactory fit.

The parameters obtained by excluding the Σ, F optical branch are shown in Table III. The curves drawn in Fig. 6 are calculated using the five-parameter set 2. The dashed parts of the curves were not observed, and calculations, in fact, show that the dynamical structure factor is vanishing in those regions, as referred to the 111 reciprocal-lattice point.

The actual values of the exchange constants are somewhat dependent, of course, upon whether some data are excluded or not, but the qualitative picture of the coupling in CrBr$_3$ one gets from Table III is independent of it.

As is expected for geometrical reasons J_1, the nearest-neighbor coupling within the honeycomb layers, is by far the dominant interaction, which is primarily responsible for the ferromagnetic ordering within the layers. A small antiferromagnetic contribution is indicated by the third-neighbor coupling J_3. One should note that relative to the

two-parameter model[6,7] a relation $J_T \rightarrow J_1 + 2J_3$ is not valid. An approximate relation can be found only by comparing the expanded energy expressions.

The interlayer interactions J_2, J_4, and J_5 are all of the same order of magnitude and are much weaker than J_1, also in agreement with what one would expect from geometrical arguments. Geometrically, J_4 and J_5 are almost equivalent and the fit is not much influenced by restricting them to be equal. These two interactions are weak because they act via two intervening Br$^-$ ions. That is also the case for J_2, but here there are more Cr^{3+}-Br$^-$-Cr^{3+} links possible, and the geometry is somewhat different. It is a most interesting result that J_2 turns out to be antiferromagnetic. The effective interlayer coupling, which for the two-parameter model is J_L, is therefore ferromagnetic because the three J_4 and six J_5 interactions outweight the one J_2. This balance may well be affected by geometrical changes throughout the chromium-trihalide series, giving a clue to understanding why CrCl$_3$ is antiferromagnetic and CrI$_3$ is a ferromagnet with a higher Curie point.[22] Again, a relation between J_L and the actual interactions is not simply $J_L \rightarrow \frac{1}{2}(J_2 + 3J_4 + 6J_5)$, although this is a fair approximation for the Λ direction (see Sec. VI).

For the calculated curves of Fig. 6, one notices, of course, the pronounced disagreement with observation for the Σ, F optical branch.

We shall now discuss briefly some possible reasons for this discrepancy. It should first be pointed out, however, that the Σ optical branch was tested for temperature effects by following one point up to the Curie temperature. As for spin waves of lower energies, a modest renormalization with increasing temperature was seen, and the peak disappeared above T_C by broadening. Furthermore, some scans were performed across the energies of the calculated Σ optical curve of Fig. 6, but no indications of peaks there were seen. We therefore conclude that the observed Σ branch is the optical spin-wave branch.

We think the most likely explanation of the discrepancy is that the optical Σ spin waves interact strongly with some other excitations, the most

TABLE III. Values in meV of coupling parameters of Table I and Eqs. (A7) and (A8) as obtained from least-squares fitting to the observed dispersion relation at 6 °K. No temperature correction has been applied. The minimized function F_{min} is so defined (Ref. 16) that it would approach a value of about unity for a statistically acceptable fit. Notice that fit 1 includes the optical branch [94 SW (spin waves)], whereas fits 2 and 3 do not (70 SW). Fit 3 is restrained by requiring $J_4 = J_5$.

No. of fit	Data	$E_g = \mu g H_A$	J_1	J_2	J_3	J_4	J_5	F_{min}	
1	94 SW	0.08	0.727	0.0071	-0.0466	0.0153	0.0185	5.77	Systematic deviations
2	70 SW	0.08	0.849	-0.0240	-0.0143	0.0068	0.0130	0.721	Optical branch
3	70 SW	0.08	0.849	-0.0239	-0.0117	0.0106	0.0106	0.732	not included
Uncertainties		0.02	0.012	0.0030	0.0060	0.0040	0.0040		$|J_6|$ and $|J_7| < 0.002$

obvious candidates being optical phonons. The
fact that we did not see any phonons in the actual
energy range does not exclude them from being
there, since the experiment was not designed for
observation of phonons. A separate experiment
to settle this point is obviously needed. Some
acoustical phonons were looked for at the 444
reciprocal-lattice point; TA(Σ, Δ) with energy
slope of 11 meV$\overset{\circ}{\text{A}}$ and LA(Λ) with energy slope
14 meV$\overset{\circ}{\text{A}}$ were seen.

The possibility should be considered that the
ground state may not be truly ferromagnetic. A
canted or cone-structure ground state that easily
aligns ferromagnetically in fields applied for mag-
netization and resonance measurements is not
ruled out by present experimental evidence. We
have, however, not seen any indication in our work
of the occurrence of satellite neutron peaks, to
which a cone structure would give rise, but again
we did not particularly look for them. If the ground
state is not ferromagnetic, one does not expect a
good fit to the theoretical expressions of the
Appendix. Antiferromagnetic ordering of the same
type as in $CrCl_3$, as has been indicated by some
workers,[23] is ruled out by the presence of magnetic
contribution to the (001) elastic reflection.

VIII. TEMPERATURE EFFECTS ON SPIN WAVES

Spin waves can be considered as strictly nonin-
teracting only at absolute zero temperature.[2,24]
At finite temperatures they are no longer perfect
modes, and this is manifest in two ways in a neutron
experiment. First, the spin-wave energy is re-
normalized, i.e., the observed center of gravity
of the neutron peaks shifts to lower energies with
increasing temperature, and second the lifetime
is decreased, which may cause a broadening of
the neutron peak widths.

The observed renormalization is illustrated in
Fig. 4, which shows peaks at two temperatures of
spin waves of comparable energies propagating in
the Σ, Δ (basal-plane) and the Λ (c-axis) directions.
The shift of the peak positions with temperature is
noticed. The most interesting feature of Fig. 4
is, however, the pronounced directional dependence
of the energy shift: The Λ spin waves renormalize
much more strongly than those along Σ, Δ. Such
an effect has been predicted theoretically for $CrBr_3$,[7]
and is caused by a stronger spin-wave–spin-wave
interaction along the direction where the dispersion
relation is flat. In order to facilitate a detailed
direct comparison with theories, we have sub-
tracted the experimentally determined[19] tempera-
ture dependence of the energy gap $E_g(T)$ from the
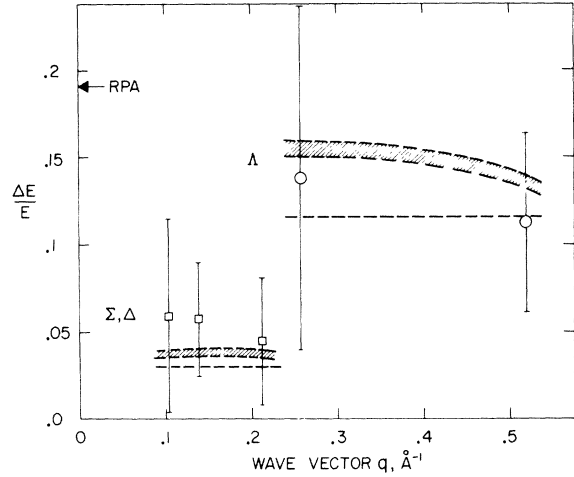observed shifts and presented the data in Fig. 7
in the form

FIG. 7. Observed and predicted relative energy
shifts $\Delta E/E$ of Eq. (1) between 4.6 and 20 °K for various
low-energy spin waves. One notices that the shifts are
larger for the Λ direction than for Σ, Δ, in agreement
with predictions of the two Dyson-type theories: The
Born approximation (Ref. 7) (dashed horizontal lines)
and the t-matrix calculations (Ref. 8) (shaded bands,
where the bandwidths indicate the numerical uncertain-
ties). The random-phase approximation would predict
a constant shift of $\Delta E/E = 0.192$ for all the spin waves.

$$\frac{\Delta E}{E} = \frac{[E(4.6\ °\text{K}) - E_g(4.6\ °\text{K})] - [E(20\ °\text{K}) - E_g(20\ °\text{K})]}{E(4.6\ °\text{K}) - E_g(4.6\ °\text{K})} . \tag{1}$$

Three different theoretical predictions of this
quantity are also shown in Fig. 7. The three theories
take the spin-wave interaction into account to dif-
ferent degrees of sophistication: (i) the random-phase
approximation (RPA), (ii) the low-density spin-wave
expansion to first order in the interaction (the first
Born approximation), and (iii) the full summation of
the Born series for first order in the density and to
all orders in the interaction (the full t matrix).[25]
The RPA is known to represent an oversimplifica-
tion, giving rise to a T^3 term in the magnetization
variation. The latter two theories yield Dyson's
T^4 term, but only the t matrix calculation gives
the proper coefficient.[24,25] For the energy shift,
the RPA predicts a $\Delta E/E$ proportional to the average
magnetization and independent of wave vector, which
is far from being the case, as seen in Fig. 7. The
experimental data are, on the contrary, in full
agreement with the Dyson-type theories, giving for
the first time, direct evidence for the spin-wave
"renormalization by the energy"[26] by demonstrating
its directional dependence. Similar direct evidence
is very hard to obtain experimentally for systems
lacking the strong directional dependence of the
spin-wave energy found in $CrBr_3$. The measured
energy shifts are too small to distinguish between
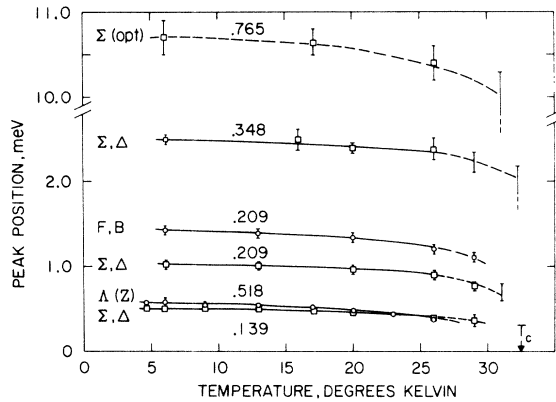the Born approximation[7] and the t-matrix[8] calcula-

FIG. 8. Variation with temperature of the energy of various spin waves. Broadened peaks near T_C are shown as vertical bars. Where fully drawn, the curves are calculations with the Born approximation (Ref. 7), taking the temperature variation of the energy gap E_g into account. Notice the break of the energy scale to show one optical spin wave. The spin waves are labeled by directions and values of wave vectors q in Å^{-1}.

tions, however. These calculations were performed with the two-parameter lattice model, using the values of J_L and the average J_T as determined from the neutron measurements. In fact, to make the t-matrix calculations feasible, a rectangular model was used.[8] It was tested against the honeycomb model by comparing the results of the Born-approximation calculations for the two models, and for practical purposes the results were identical.

In Fig. 8, we show more explicitly the energy shifts vs. temperature for various spin waves, as labeled by their directions and wave vectors. A part of the shift is caused by the temperature variation of the energy gap $E_g(T)$. The remaining effect, being due to interactions among spin waves, can be calculated theoretically for temperatures not too close to T_C. The RPA would give a variation like the magnetization, which is not at all the case in Fig. 8. The two Dyson theories give almost identical results on the scale of the figure and the curves are those calculated with the Born approximation and including the known variation of $E_g(T)$.[19] Calculated renormalization of the optical branch is not included since its low-temperature dispersion is somewhat anomalous, as explained in Sec. VII.

The peak broadening or lifetime effect is too small compared to the instrumental resolution to be determined for temperatures below about 25 °K. As the Curie point is approached, however, the peak widths increase quite rapidly and in fact the peaks disappear at T_C by broadening out rather than renormalizing to zero energy. This effect resembles the behavior of the spin waves in the two-dimensional

antiferromagnet K_2NiF_4,[27] in particular for the basal plane where the renormalization is weakest. In two-dimensional systems, the spin waves persist to higher temperatures relative to the transition point than for traditional three-dimensional systems, and this is so because the transition temperature is lowered by the weakness of the third-dimensional coupling. Accordingly, the validity of the spin-wave theory is not determined by the smallness of the parameter T/T_C but rather of $k_B T/2SzJ_1$, where z is the number of neighbors with the strongest interaction J_1. This explains why the renormalization calculation of Fig. 8 evidently works well up to above $0.8T_C$, although it is based on a low-density expansion.

The t-matrix theory also predicts the peak broadening effect correctly (as being small) up to this same temperature range. Nearer T_C multiple spin-wave scattering becomes increasingly important, however, and, in fact, no reliable theory for the peak broadening exists where it is experimentally observable.

APPENDIX

We shall here give the expressions for the dispersion relation of free spin waves in ferromagnetic $CrBr_3$. An isotropic Heisenberg Hamiltonian

$$\mathcal{H} = - \sum_{\substack{nn' \\ jj'}} J_{nn'jj'} \, \vec{S}_{nj}\vec{S}_{n'j'} - \mu_B g H_A \sum_{nj} S_{nj}^z \tag{A1}$$

is assumed with exchange parameters $J_m = J_{nn'jj'}$ between Cr^{3+} ions of mth nearest neighbors, connecting the spins in unit cells n and n' on sublattices j and j', respectively. H_A is an effective anisotropy field, acting along the average spin direction, and like the g factor, assumed equal for both sublattices.

The dispersion relation for spin waves in the simplified lattice[6,7] involving two interaction parameters J_T and J_L was derived in Ref. 7. For propagation along the Λ direction (c axis) the relation reads

$$E_L(q) = E_g + 6J_T S(1 \mp 1) + 4J_L S[1 - \cos(c_H \times \tfrac{1}{3}q)],$$

$$\tag{A2}$$

where $E_g = \mu_B g H_A$, S is the spin value ($= \tfrac{3}{2}$ for Cr^{3+}), and $c_H = 18.26$ Å is the hexagonal c-axis parameter. The upper sign ($-$) corresponds to the acoustical branch, and the lower sign ($+$) corresponds to the optical branch.

For propagation within the basal plane the dispersion relation reads

$$E_T = E_g + 6 J_T S \left[1 \mp \tfrac{1}{3} (\gamma_q \, \gamma_{-q})^{1/2} \right] . \tag{A3}$$

For the Σ direction (coinciding with the shortest Cr-Cr bond), one finds

$$\gamma_q \gamma_{-q} = 5 + 4 \cos(\sqrt{3} \, a_H \times \tfrac{1}{2} q), \tag{A4}$$

and for the Δ direction (normal to Σ),

$$\gamma_q \gamma_{-q} = 1 + 4 [1 + \cos(a_H \times \tfrac{1}{2} q)] \cos(a_H \times \tfrac{1}{2} q) , \tag{A5}$$

where $a_H = 6.26 \text{Å}$ is the hexagonal a-axis parameter. Evaluations of the cosine functions show that the energy is practically identical along the two directions for $q < 0.35 \text{Å}^{-1}$, showing that the basal-plane spin waves of Fig. 5 can be described equally well by any of Eqs. (A4) and (A5), although the quadratic expansion is valid only for $q \lesssim 0.15 \text{Å}^{-1}$.

The dispersion relation for spin waves in the actual BiI_3-type lattice was derived from Eq. (A1) using standard methods[11] and allowing for up to a seventh-neighbor interaction. With the interaction parameters of Table I the expressions are

$$E(\vec{q}) = A(\vec{q}) \mp B^{1/2}(\vec{q}), \tag{A6}$$

where

$$A(\vec{q}) = E_g + 2S[3J_1 + J_2 + 3J_4 + 3J_6 + 6J_7$$
$$+ 2J_3(3 - W_c) + 2J_5(3 - V_c)], \tag{A7}$$

$$B(\vec{q}) = 4 S^2 \{ (J_1^2 + J_4^2)(3 + 2W_c) + (J_2 + 2J_7 W_c)^2$$
$$+ J_6^2 (3 + 2W_{2c}) + 2J_1 [J_4(2V_c + U_c)$$

$$+ J_6 (W_{cp} + 2P_c) + (J_2 + 2J_7 W_c) V_c]$$
$$+ 2(J_2 + 2J_7 W_c) (J_4 W_{cp} + J_6 U_c)$$
$$+ 2J_4 J_6 (2W_c Z_c + Q_c) \} , \tag{A8}$$

and the following functions of the wave vector $\vec{q}$ and the rhombohedral unit vectors $\vec{t}_1, \vec{t}_2,$ and $\vec{t}_3$ have been introduced through the variables

$$\alpha = \vec{q} \cdot \vec{t}_1,$$
$$\beta = \vec{q} \cdot \vec{t}_2, \tag{A9}$$
$$\gamma = \vec{q} \cdot \vec{t}_3 ;$$

$$U_c = \cos(\alpha + \beta - \gamma) + \cos(\beta + \gamma - \alpha) + \cos(\gamma + \alpha - \beta),$$

$$V_c = \cos\alpha + \cos\beta + \cos\gamma ,$$

$$W_c = \cos(\alpha - \beta) + \cos(\beta - \gamma) + \cos(\gamma - \alpha),$$

$$W_{cp} = \cos(\alpha + \beta) + \cos(\beta + \gamma) + \cos(\gamma + \alpha), \tag{A10}$$

$$W_{c2} = \cos2(\alpha - \beta) + \cos2(\beta - \gamma) + \cos2(\alpha - \gamma),$$

$$Z_c = \cos(\alpha + \beta + \gamma),$$

$$P_c = \cos2\alpha \cos(\beta - \gamma) + \cos2\beta \cos(\gamma - \alpha)$$
$$+ \cos(2\gamma) \cos(\alpha - \beta),$$

$$Q_c = \cos[2(\alpha + \beta) - \gamma] + \cos[2(\beta + \gamma) - \alpha]$$
$$+ \cos[2(\gamma + \alpha) - \beta].$$

The minus sign in Eq. (A6) gives the acoustical branch and the plus sign the optical branch.

*Guest Scientist from Institutt for Atomenergi, Kjeller, Norway, now returned.

†Work performed under the auspices of the U. S. Atomic Energy Commission.

[1] C. Herring, in *Magnetism IIb*, edited by T. Rado and H. Suhl (Academic, New York, 1966), p. 1.

[2] F. Keffer, in *Handbuch der Physik*, edited by S. Flügge (Springer, Berlin, 1966), Vol. XVIII, Chap. 2, p. 1.

[3] Extended reference lists to the literature prior to 1965 are given in Keffer's review article, Ref. 2.

[4] See, for instance, R. D. Lowde, J. Appl. Phys. **36**, 884 (1965).

[5] I. Tsubokawa, J. Phys. Soc. Japan **15**, 1664 (1960).

[6] A. C. Gossard, V. Jaccarino, and J. P. Remeika, Phys. Rev. Letters **7**, 122 (1961).

[7] H. L. Davis and A. Narath, Phys. Rev. **134**, A433 (1964).

[8] R. Silberglitt, C. H. Cobb, and V. Jaccarino, J. Appl. Phys. **41**, 952 (1970).

[9] A. Braekken, Kgl. Norske Videnskab. Selskabs Forh. **5**, 173 (1932).

[10] B. Morisin and A. Narath, J. Chem. Phys. **40**, 1958 (1964).

[11] A. W. Sáenz, Phys. Rev. **125**, 1940 (1962).

[12] R. W. Bené, Phys. Rev. **178**, 497 (1969).

[13] P. A. Lindgard, A. Kowalska, and P. Laut, J. Phys. Chem. Solids **28**, 1357 (1967).

[14] G. F. Koster, Solid State Phys. **5**, 173 (1957).

[15] M. J. Cooper and R. Nathans, Acta Cryst. **23**, 357 (1967).

[16] E. J. Samuelsen, M. T. Hutchings, and G. Shirane, Physica **48**, 13 (1970).

[17] H. Watanabe and B. N. Brockhouse, Phys. Letters **1**, 189 (1962).

[18] E. J. Samuelsen and G. Shirane, Phys. Status Solidi (to be published).

[19] J. F. Dillon, Jr., J. Appl. Phys. **33**, 1191S (1962).

[20] The conversion factors of units are 1 meV = 11.60 °K = 8.067 cm^{-1}.

[21] C. H. Cobb, V. Jaccarino, and R. Silberglitt (private communication). The problems associated with attempting to fit experimental data on both the temperature and field dependence of the magnetization with the simplified lattice will be discussed by these authors in a future publication.

[22] Pertinent data for the three compounds are tabulated by J. F. Dillon, Jr., H. Kamimura, and J. P. Remeika, J. Phys. Chem. Solids **27**, 1531 (1966).

[23] H. Bizette and C. Terrier, J. Phys. **23**, 486 (1962).

[24] F. J. Dyson, Phys. Rev. **102**, 1217 (1956); **102**, 1230 (1956).

[25] R. Silberglitt and A. B. Harris, Phys. Rev. **174**, 640 (1968).

[26] F. Keffer and R. Loudon, J. Appl. Phys. **32**, 2S (1961); **33**, 250 (1962).

[27] R. J. Birgeneau, J. Skalyo, Jr., and G. Shirane, J. Appl. Phys. **41**, 1303 (1970).